IMPORTANT NOTICE: The current official version of this document is available via the Sandia National Laboratories WIPP Online Documents web site. A printed copy of this document may not be the version currently in effect.

SANDIA NATIONAL LABORATORIES
WASTE ISOLATION PILOT PLANT

AP-179
Revision 0

Analysis Plan for
Modifications to the Munson-Dawson Model

Task 4.4.2.4.1

Effective Date: September 20, 2017

Authored by:	Benjamin Reedlunn	*Original signed by Shelly R. Nielsen for*	*9-19-17*
	Print Name	Signature	Date
Reviewed by:	Courtney Herrick	*Original signed by Shelly R. Nielsen for*	*9-19-17*
	Print Name Technical Reviewer	Signature	Date
Reviewed by:	Shelly R. Nielsen	*Original signed by Shelly R. Nielsen*	*9-19-17*
	Print Name Quality Assurance Reviewer	Signature	Date
Approved by:	Christi D. Leigh	*Original signed by Christi D. Leigh*	*9-19-17*
	Print Name Department Manager	Signature	Date

© 2017 NTES of Sandia, LLC.

Table of Contents

1 Introduction and Objectives 3
1.1 Current Munson-Dawson Model 3
1.2 Shortcomings of the Munson-Dawson Model 5
1.2.1 Creep at Low Equivalent Stresses 5
1.2.2 Equivalent Stress Measure 6
1.2.3 Numerical Robustness 7
1.2.4 Damage, Fracture, and Healing 8
2 Approach 8
2.1 Initial Modifications 8
2.1.1 Creep at low equivalent stresses 8
2.1.2 Equivalent stress measure 9
2.1.3 Numerical Robustness 9
2.2 Larger Modifications 10
3 Software List 10
4 Tasks 10
5 Special Considerations 10
6 Applicable Procedures 11
7 References 11

1 Introduction and Objectives

Sandia National Laboratories currently uses the Munson-Dawson model (also known as the MD or Multimechanism Deformation model) (Munson et al., 1989) to simulate the thermo-mechanical behavior of rock salt. While the MD model has its strengths, it currently

1. fails to capture the creep behavior at low equivalent stresses,
2. does not agree well with tri-axial creep experiments at multiple Lode angles,
3. needs improvements to its numerical implementation,
4. cannot model diffuse microstructural damage,
5. cannot model macroscopic fractures, and
6. cannot model healing (damage reduction).

This analysis plan outlines a path to resolve these shortcomings by modifying the model in Sierra/Solid Mechanics. The analysis proposed herein will be used for Programmatic Decisions, per NP 9-1 *Analyses*.

1.1 Current Munson-Dawson Model

The MD model has evolved over the years (Munson and Dawson, 1979, 1982; Munson et al., 1989), so it is worthwhile to explicitly define the current model formulation before discussing its shortcomings and how one might resolve them. Please note that a slightly different notation is used than in previous presentations (Munson et al., 1989; Munson, 1997; Rath and Argüello, 2012), but the equations are the same.

The MD model is an isotropic, hypoelastic, viscoplastic material model. The total strain rate $\dot{\boldsymbol{\varepsilon}}$ is decomposed into an elastic strain rate $\dot{\boldsymbol{\varepsilon}}^{\mathrm{el}}$, a thermal strain rate $\dot{\boldsymbol{\varepsilon}}^{\mathrm{th}}$, and a viscoplastic strain rate $\dot{\boldsymbol{\varepsilon}}^{\mathrm{vp}}$:

$$\dot{\boldsymbol{\varepsilon}} = \dot{\boldsymbol{\varepsilon}}^{\mathrm{el}} + \dot{\boldsymbol{\varepsilon}}^{\mathrm{th}} + \dot{\boldsymbol{\varepsilon}}^{\mathrm{vp}}. \tag{1.1}$$

(As is common in the geomechanics literature, compressive strains and stresses are treated as positive.) The hypoelastic portion of the M-D model utilizes the following simple linear relationship between the elastic strain rate $\dot{\boldsymbol{\varepsilon}}^{\mathrm{e}}$ and the stress rate $\dot{\boldsymbol{\sigma}}$,

$$\dot{\boldsymbol{\sigma}} = \boldsymbol{\mathcal{C}} : \dot{\varepsilon}^{\mathrm{el}} \tag{1.2}$$

$$\boldsymbol{\mathcal{C}} = (B - 2/3\,\mu)\,\boldsymbol{I} \otimes \boldsymbol{I} + 2\,\mu\,\boldsymbol{\mathcal{I}}, \tag{1.3}$$

where $\boldsymbol{\mathcal{C}}$ is the fourth-order elastic stiffness tensor composed of the bulk modulus B, the shear modulus μ, the second-order identity tensor $\boldsymbol{I}$, and the forth-order symmetric identity tensor $\boldsymbol{\mathcal{I}}$. The thermal strain portion of the model is simply

$$\dot{\boldsymbol{\varepsilon}}^{\mathrm{th}} = \alpha\,\dot{T}\,\boldsymbol{I} \tag{1.4}$$

where α is the coefficient of thermal expansion, and T is the temperature. The viscoplastic portion of the model captures the stress, time, and temperature dependence of plastic deformation. Plastic deformation of intact salt is isochoric and only occurs in the presence of shear stress. The M-D model's measure of shear stress is the Tresca equivalent stress

$$\bar{\sigma} = \max\left(|\sigma_1 - \sigma_2|,\ |\sigma_2 - \sigma_3|,\ |\sigma_3 - \sigma_1|\right), \tag{1.5}$$

where σ_i are the principal stresses. The viscoplastic strain evolves according to an associated flow rule

$$\dot{\boldsymbol{\varepsilon}}^{\mathrm{vp}} = \dot{\bar{\varepsilon}}^{\mathrm{vp}} \frac{\partial \bar{\sigma}}{\partial \boldsymbol{\sigma}}, \tag{1.6}$$

where $\dot{\bar{\varepsilon}}^{\mathrm{vp}}$ is the equivalent viscoplastic strain rate. It can be decomposed into two components

$$\dot{\bar{\varepsilon}}^{\mathrm{vp}} = \dot{\bar{\varepsilon}}^{\mathrm{tr}} + \dot{\bar{\varepsilon}}^{\mathrm{ss}}, \tag{1.7}$$

where $\dot{\bar{\varepsilon}}^{\mathrm{tr}}$ is the transient equivalent viscoplastic strain rate and $\dot{\bar{\varepsilon}}^{\mathrm{ss}}$ is the steady state equivalent viscoplastic strain rate.

The steady state behavior is modeled as a sum of three mechanisms, each of which vary with stress and temperarture:

$$\dot{\bar{\varepsilon}}^{\mathrm{ss}} = \sum_{i=1}^{3} \dot{\bar{\varepsilon}}_i^{\mathrm{ss}}, \tag{1.8}$$

where

$$\dot{\bar{\varepsilon}}_1^{\mathrm{ss}} = A_1 \exp\left(-\frac{Q_1}{RT}\right) \left(\frac{\bar{\sigma}}{\mu}\right)^{n_1}, \tag{1.9}$$

$$\dot{\bar{\varepsilon}}_2^{\mathrm{ss}} = A_2 \exp\left(-\frac{Q_2}{RT}\right) \left(\frac{\bar{\sigma}}{\mu}\right)^{n_2}, \tag{1.10}$$

$$\dot{\bar{\varepsilon}}_3^{\mathrm{ss}} = H(\bar{\sigma} - \bar{\sigma}_0) \left[B_1 \exp\left(-\frac{Q_1}{RT}\right) + B_2 \exp\left(-\frac{Q_2}{RT}\right)\right] \sinh\left(q \frac{(\bar{\sigma} - \bar{\sigma}_0)}{\mu}\right). \tag{1.11}$$

The variables A_i, B_i, Q_i, n_i, $\bar{\sigma}_0$, and q are all model parameters. All three mechanisms have an Arrhenius temperature dependence, where Q_i is an activation energy and $R = 8.314$ J/(K mol) is the universal gas constant. The first mechanism Eq. (1.9) is meant to capture dislocation climb, which dominates at high temperatures and low equivalent stresses. The second mechanism Eq. (1.10) dominates at low temperatures and low equivalent stresses. The micro-mechanical cause for the second mechanism is unknown, but cross-slip has been recently suggested (Hansen, 2014). Regardless, the macroscopic behavior corresponding to the second mechanism has been well characterized. The third mechanism Eq. (1.11) models dislocation glide, which is only activated when $\bar{\sigma}$ exceeds $\bar{\sigma}_0$, as reflected in the heaviside function $H(\bar{\sigma} - \bar{\sigma}_0)$.

The transient behavior is somewhat more complex than the steady-state because it involves an ordinary differential equation rather than the simple functional forms in Eqs. (1.9) to (1.11). During work hardening, $\bar{\varepsilon}^{\mathrm{tr}}$ approaches the transient strain limit $\bar{\varepsilon}^{\mathrm{tr}*}$ from below, and the creep strain rate slows down over time. (See Section 1.3.1 in Reedlunn (2016) for an

example.) During recovery, $\bar{\varepsilon}^{\mathrm{tr}}$ approaches $\bar{\varepsilon}^{\mathrm{tr}*}$ from above, and the creep strain rate speeds up over time. The value of $\bar{\varepsilon}^{\mathrm{tr}*}$ varies with temperature and stress as,

$$\bar{\varepsilon}^{\mathrm{tr}*} = K_0 \exp(cT) \left(\frac{\bar{\sigma}}{\mu}\right)^m, \tag{1.12}$$

where K_0, c, and m are parameters to be calibrated against experimental results. The rate that $\bar{\varepsilon}^{\mathrm{tr}}$ approaches $\bar{\varepsilon}^{\mathrm{tr}*}$ is governed by

$$\dot{\bar{\varepsilon}}^{\mathrm{tr}} = (F-1)\, \dot{\bar{\varepsilon}}^{\mathrm{ss}}, \tag{1.13}$$

where the proportionality $(F-1)$ depends on whether the material is work hardening or recovering. These two behaviors are captured in the following equations

$$F = \begin{cases} \exp\left[\kappa_{\mathrm{h}} \left(1 - \frac{\bar{\varepsilon}^{\mathrm{tr}}}{\bar{\varepsilon}^{\mathrm{tr}*}}\right)^2\right] & \bar{\varepsilon}^{\mathrm{tr}} \leq \bar{\varepsilon}^{\mathrm{tr}*} \\ \exp\left[-\kappa_{\mathrm{r}} \left(1 - \frac{\bar{\varepsilon}^{\mathrm{tr}}}{\bar{\varepsilon}^{\mathrm{tr}*}}\right)^2\right] & \bar{\varepsilon}^{\mathrm{tr}} > \bar{\varepsilon}^{\mathrm{tr}*}. \end{cases} \tag{1.14}$$

The quantities κ_{h} and κ_{r} control how quickly the transient equivalent viscoplastic strain approaches the transient limit for a given $\dot{\bar{\varepsilon}}^{\mathrm{ss}}$. These quantities vary with equivalent stress as,

$$\kappa_{\mathrm{h}} = \alpha_{\mathrm{h}} + \beta_{\mathrm{h}} \log_{10}\left(\frac{\bar{\sigma}}{\mu}\right), \tag{1.15}$$

$$\kappa_{\mathrm{r}} = \alpha_{\mathrm{r}} + \beta_{\mathrm{r}} \log_{10}\left(\frac{\bar{\sigma}}{\mu}\right), \tag{1.16}$$

where α_j and β_j are model parameters.

1.2 Shortcomings of the Munson-Dawson Model

This section will review some of the shortcomings of the MD model, as implemented in Sierra/Solid Mechanics.

1.2.1 Creep at Low Equivalent Stresses

As previously mentioned, the MD model was recently used to simulate Room D, and the simulation under predicted the vertical closure by 3.1× at 3.7 years (Reedlunn, 2016). Several causes for the under predictions have been proposed, but the failure to capture the creep behavior at low equivalent stresses is near the top of the list. Figure 1.1 compares experimental measurements of the steady-state strain rate and transient strain limit against a calibration of the MD model (Cal 1B) at various equivalent stresses and temperatures. The experimental measurements at $T = 60$ °C exhibit what appears to be bi-linear behavior, changing slope at about $\bar{\sigma} = 8$ MPa. Higher than expected $\dot{\bar{\varepsilon}}^{\mathrm{ss}}$ values at low equivalent

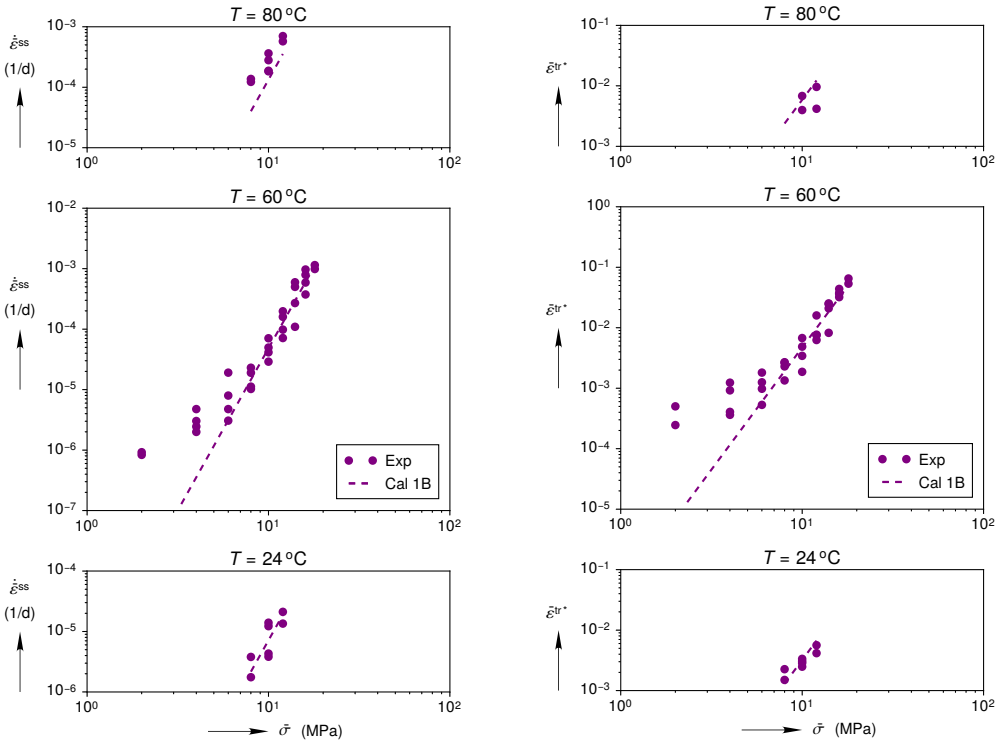

(a) Steady-State Strain Rate (b) Transient Strain Limit

Figure 1.1: Calibration 1B compared against experiments (Reedlunn, 2016).

stresses have been previously observed (Bérest et al., 2005, 2015), but these are the first measurements of $\bar{\varepsilon}^{\mathrm{tr}*}$ values at low equivalent stresses. A new micro-mechanical mechanism for creep may be activated at these low equivalent stresses. (In fact, an attempt to identify the mechanism is planned under Test Plan 17-04 "Microstructural Investigations on Natural and Laboratory Tested Salt" (Mills, 2017).) The M-D model in its present form is incapable of capturing this bi-linear behavior. One could combine steady-state strain rate mechanism 1 and mechanism 2 (Eqs. (1.9) and (1.10)) to model the low and high equivalent stress regimes, but then mechanism 1 would not be available for modeling dislocation climb at high temperatures. More importantly, the transient strain limit relation (Eq. (1.12)) simply cannot capture both low and high equivalent stress regimes.

1.2.2 Equivalent Stress Measure

The MD model originally used a von Mises equivalent stress, without any facets or sharp corners, but the equivalent stress measure was changed to Tresca in Munson et al. (1989). As shown in the π-plane plot in Fig. 1.2, the maximum difference between these two equivalent stress measures is only 15.5 %, so one might not expect a large impact on room closure. This difference, however, gets amplified by the exponents in Eqs. (1.9) to (1.12). For example, typically $n_2 \approx 5$, so a 15.5 % increase in $\bar{\sigma}$ causes a 2.05× increase in $\dot{\bar{\varepsilon}}_2^{\mathrm{ss}}$. Munson et al. (1989) justified the switch to the Tresca equivalent stress by inspecting measurements on hollow

cylinders of Avery Island rock salt subjected to axial compression, internal pressurization, and external pressurization[1]. Controlling these three stresses allowed the experimentalist to vary the Lode angle and measure the resulting strains. The Tresca equivalent stress matched the experimental results better than the von Mises equivalent stress, but the experimental data suggests a more accurate representation is somewhere in-between the two stress measures: a hexagonal type shape without sharp corners.

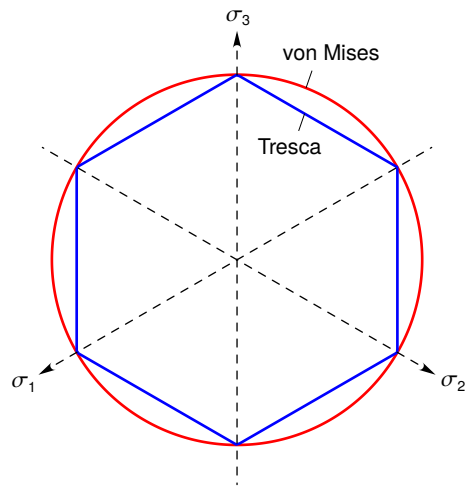

Figure 1.2: Tresca and von Mises equivalent stress surfaces compared.

1.2.3 Numerical Robustness

The Room D study also revealed that the three implementations of the MD model in Sierra/Solid Mechanics have numerical issues. The three implementations are called the `munson_dawson` model, the `md_creep` model, and the `implicit_wipp_crushed_salt` model. (The `implicit_wipp_crushed_salt` model is actually an implementation of the Callahan model for crushed salt (Callahan, 1999), but it reduces down to the MD model when the density matches that of intact salt.) The `munson_dawson` model integrates the ordinary differential equations explicitly using the forward Euler method (Weatherby et al., 1996). When the host finite element code calls the `munson_dawson` model, the `munson_dawson` model uses the supplied rate of deformation and supplied time step to calculate a critical time step. If the supplied time step is less than the critical time step, then explicit integration can proceed without numerical instabilities. If the supplied time step is larger than the critical time step, then the model sub-divides the time step into smaller time steps equal to or less than the critical time step so it can explicitly integrate through the sub time steps. This approach is acceptable if the deformation increment is sufficiently small, but the host finite element code

[1]Munson et al. (1989) cites a manuscript titled "Multiaxial Creep of Natural Rock Salt" submitted to the International Journal of Plasticity in 1989 for the full experimental details on the hollow cylinder tests. It appears this particular manuscript was never published. Mellegard et al. (1992), however, contains the hollow cylinder results Munson et al. (1989) refers to.

infrequently will supply a large rate of deformation to a material point. If the latter happens, the `munson_dawson` model will compute an extremely small critical time step relative to the supplied time step, resulting in excessively long computation times. Simulations can "stop" for hours while the problematic material point integrates the constitutive equations. The `md_creep` and `implicit_wipp_crushed_salt` models avoid the extremely small critical time step issue by using an implicit, backward Euler, scheme to integrate its constitutive equations. In practice, the `md_creep` and `implicit_wipp_crushed_salt` models often finished simulations faster than the `munson_dawson` model, but the implicit algorithm struggled to converge, causing numerous time step cut backs. The precise causes for the convergence failures have not been tracked down, but the faceted shape and sharp corners of the MD model's Tresca equivalent stress (see Fig. 1.2) are probably important.

1.2.4 Damage, Fracture, and Healing

The current MD model can only model elastic and viscoplastic deformation. Salt, however, can also develop microcracks that reduce its load carrying capacity and increase its permeability to fluid flow. Microcracks (also known as damage) form due to viscoplasticity under low confinement conditions, which often occurs to the salt surrounding a drift. If left unchecked, microcracks will eventually coalesce into macrocracks. Under high confinement condtions, however, the microcracks will heal due to pressure solution redeposition. An accurate prediction of damage, fracturing, and healing helps simulate the waste encapsulation process, the effectiveness of the seal systems, and the structural performance of the repository. The Munson-Dawson-Chan-Fossum model (also known as the MDCF or Multimechanism Deformation Coupled Fracture model) was developed to add damage, fracturing, and healing to the MD model (Chan et al., 1998), but it was never implemented in Sierra/Solid Mechanics, so the MD model remains the starting point herein.

2 Approach

The initial modifications to the MD model will probably be the creep at low equivalent stresses, the equivalent stress definition, and the numerical implementation. Once these more limited issues have been satisfactorily resolved, the focus can shift to capturing damage, fracturing, and healing. All modifications will be clearly documented, including the numerical implementation.

2.1 Initial Modifications

2.1.1 Creep at low equivalent stresses

The creep at low equivalent stresses will likely be captured by simply adding new terms to the steady state strain rate and the transient strain limit. Unless new information on the micromechanism behind creep at low equivalent stresses comes to light, the new terms will

probably be similar to the existing terms. For example, a new steady-state term of the form

$$\dot{\bar{\varepsilon}}_0^{\mathrm{ss}} = A_0 \, \exp\left(-\frac{Q_0}{RT}\right) \left(\frac{\bar{\sigma}}{\mu}\right)^{n_0} \tag{2.1}$$

may be added to the sum in Eq. (1.8), and a new transient strain limit of the form

$$\bar{\varepsilon}^{\mathrm{tr}*} = \sum_{i=0}^{1} K_i \, \exp(c_i \, T) \left(\frac{\bar{\sigma}}{\mu}\right)^{m_i} \tag{2.2}$$

may replace Eq. (1.12). These new terms should make the MD model flexible enough to capture the experimental measurements shown in Fig. 1.1.

2.1.2 Equivalent stress measure

The equivalent stress measure will be changed from Tresca to something that improves predictions of true tri-axial creep experiments. One stress measure under consideration is

$$\bar{\sigma} = \left\{ \frac{1}{2} \left[|\sigma_1 - \sigma_2|^\eta + |\sigma_2 - \sigma_3|^\eta + |\sigma_1 - \sigma_3|^\eta \right] \right\}^{1/\eta}, \tag{2.3}$$

where $1 \leq \eta \leq \infty$. This definition for $\bar{\sigma}$ was proposed by Hosford (1972) because it encompasses the Tresca stress ($\eta = 1$ or ∞), the von Mises stress ($\eta = 2$ or 4), and a range of behaviors in between. The exponent η will most likely be calibrated against the hollow cylinder experiments in Mellegard et al. (1992).

2.1.3 Numerical Robustness

Numerical robustness should be improved by avoiding the sharp corners of the Tresca equivalent stress measure, but the algorithm for integrating the equations plays a large role as well. Explicit algorithms perform well when small strain increments are applied to the model, while implicit algorithms are supposed to fare better with large strain increments (see Section 1.2.3). The fastest approach might be to integrate the equations explicitly for small strain increments and integrate them implicitly for large strain increments, but it might be sufficient to simply implement a robust implicit algorithm.

Scherzinger (2016) recently compared the classic Newton algorithm with a Line Search algorithm for integrating the rate independent plasticity equations. Scherzinger (2016) used the equivalent stress given by Eq. (2.3) with $\eta = 6$, 8, and 100. These values of η caused the equivalent stress surface to be a hexagon with highly rounded corners, a hexagon with moderately round corners, and a hexagon with sharp corners. The Newton algorithm converged if the trial stress state was near the equivalent stress surface, but it's performance rapidly deteriorated with increasing trial stress and/or increasing η. The Line Search algorithm, on the other hand, converged in all cases.

2.2 Larger Modifications

Damage, fracturing, and healing are viewed as involved extensions to the MD model. Consequently, the published literature will be surveyed to determine an appropriate way to capture these phenomena. In addition to exploring the available experimental data, existing models will be studied for inspiration. Some of the models under consideration include the MDCF model (Chan et al., 1998), the Composite Dilatancy Model (Hampel, 2015), the Günther-Salzer model (Günther and Salzer, 2012), and the Lux/Wolters model (Blanco-Martín et al., 2016).

3 Software List

Commercial off-the-shelf (COTS) software may be used in the development of the analysis report including, but not limited to Access®, Excel®, Grapher®, Kaleidagraph®, MATHEMATICA®, MATHCAD®, MATLAB®, or Python running on workstations. The use of any COTS application will be documented and verified per Nuclear Waste Management Procedure NP 9-1, Section 2.2 as appropriate. Acquired software, including Sierra Mechanics, Dakota, and Cubit, may also be used in the development of the analysis report.

4 Tasks

The tasks, responsible personnel, and estimated task schedule are summarized in Table 4.1. The completion date and responsible individuals may change in the future.

Table 4.1: Task list and estimated schedule

Task	Description	Guiding Document	Approximate Completion Date	Responsible Individuals
1	Implement the modifications listed in Section 2.1 and document them in an Analysis Report	AP-179, NP 9-1	31 JAN 2018	Benjamin Reedlunn
2	Implement the modifications listed in Section 2.2 and document them in an Analysis Report	AP-179, NP 9-1	31 JUN 2018	Benjamin Reedlunn

5 Special Considerations

None

6 Applicable Procedures

All applicable WIPP Quality Assurance procedures will be followed when conducting these analyses.

- Training of personnel will be conducted in accordance with the requirements of NP 2-1, *Qualification and Training*.
- Analyses will be conducted and documented in accordance with the requirements of NP 9-1, *Analyses*.
- All software used will meet the requirements laid out in NP 19-1, *Software Requirements* and NP 9-1, as applicable.
- The analyses will be reviewed following NP 6-1, *Document Review Process*.
- All required records will be submitted to the WIPP Records Center in accordance with NP 17-1, *Records*.
- New and revised parameters may be created as discussed in NP 9-2, *Parameters*.

7 References

Bérest, P., Béraud, J. F., Gharbi, H., Brouard, B., DeVries, K., 2015. A very slow creep test on an Avery Island salt sample. Rock Mechanics and Rock Engineering 48 (6), 2591–2602.

Bérest, P., Blum, P. A., Charpentier, J. P., Gharbi, H., Valès, F., 2005. Very slow creep tests on rock samples. International Journal of Rock Mechanics and Mining Sciences 42 (4), 569–576.

Blanco-Martín, L., Wolters, R., Rutqvist, J., Lux, K.-H., Birkholzer, J. T., 2016. Thermal–hydraulic–mechanical modeling of a large-scale heater test to investigate rock salt and crushed salt behavior under repository conditions for heat-generating nuclear waste. Computers and Geotechnics 77, 120–133.

Callahan, G. D., 1999. Crushed salt constitutive model. Tech. Rep. SAND98-2680, Sandia National Laboratories, Albuquerque, NM, USA.

Chan, K. S., Munson, D., Fossum, A., Bodner, S., 1998. A constitutive model for representing coupled creep, fracture, and healing in rock salt. In: Aubertin, M., Jr., H. R. H. (Eds.), Proc. 4th Conference on the Mechanical Behavior of Salt. Trans Tech Publications, pp. 221–234.

Günther, R., Salzer, K., 2012. Advanced strain-hardening approach: A powerful creep model for rock salt with dilatancy, strength and healing. Mechanical Behavior of Salt VII. Eds. Bérest, P., Ghoreychi, M., Hadj-Hassen, F., Tijani, M., Paris: CRC Press/Balkema, 13–22.

Hampel, A., 2015. Description of damage reduction and healing with the cdm constitutive model for the thermo-mechanical behavior of rock salt. In: Roberts, L., Mellegard, K., Hansen, F. D. (Eds.), Mechanical Behavior of Salt VIII. pp. 361–371.

Hansen, F. D., 2014. Micromechanics of isochoric salt deformation. In: 48th US Rock Mechanics/Geomechanics Symposium. American Rock Mechanics Association.

Hosford, W., 1972. A generalized isotropic yield criterion. Journal of Applied Mechanics 39 (2), 607–609.

Mellegard, K. D., Callahan, G. D., Senseny, P. E., 1992. Multiaxial creep of natural rock salt. Tech. Rep. SAND91-7083, Sandia National Laboratories, Albuquerque, NM, USA; RE/SPEC, Inc., Rapid City, SD, USA.

Mills, M., August 2017. Microstructural investigations on natural and laboratory tested salt. WIPP Test Plan 17-04 Revision 0, Sandia National Laboratories, Albuquerque, NM, USA.

Munson, D. E., 1997. Constitutive model of creep in rock salt applied to underground room closure. International Journal of Rock Mechanics and Mining Sciences 34 (2), 233–247.

Munson, D. E., Dawson, P., 1979. Constitutive model for the low temperature creep of salt (with application to WIPP). Tech. Rep. SAND79-1853, Sandia National Laboratories, Albuquerque, NM, USA.

Munson, D. E., Dawson, P., 1982. Transient creep model for salt during stress loading and unloading. Tech. Rep. SAND82-0962, Sandia National Laboratories, Albuquerque, NM, USA.

Munson, D. E., Fossum, A. F., Senseny, P. E., 1989. Advances in resolution of discrepancies between predicted and measured in situ WIPP room closures. Tech. Rep. SAND88-2948, Sandia National Laboratories, Albuquerque, NM, USA.

Rath, J. S., Argüello, J. G., 2012. Revisiting historical numerical analyses of the waste isolation pilot plant (WIPP) Room B and D in-situ experiments regarding thermal and structural response. Tech. Rep. SAND2012-7525, Sandia National Laboratories, Albuquerque, NM, USA.

Reedlunn, B., October 2016. Reinvestigation into closure predictions of Room D at the Waste Isolation Pilot Plant. Tech. Rep. SAND2016-9961, Sandia National Laboratories, Albuquerque, NM, USA.

Safley, L. E., December 2012. Analyses. WIPP Nuclear Waste Management Procedure 9-1 Revision 9, Sandia National Laboratories, Carlsbad, NM, USA.

Scherzinger, W. M., 2016. A return mapping algorithm for isotropic and anisotropic plasticity models using a line search method. Computer Methods in Applied Mechanics and Engineering.

Weatherby, J., Munson, D., Argüello, J., 1996. Three-dimensional finite element simulation of creep deformation in rock salt. Engineering computations 13 (8), 82–105.

This work of authorship was prepared as an account of work sponsored by an agency of the United States Government. Accordingly, the United States Government retains a nonexclusive, royalty-free license to publish or reproduce the published form of this contribution, or allow others to do so for United States Government purposes. Neither the National Technology and Engineering Solutions of Sandia, LLC., the United States Government, nor any agency thereof, nor any of their employees makes any warranty, express or implied, or assumes any legal liability or responsibility for the accuracy, completeness, or usefulness of any information, apparatus, product, or process disclosed, or represents that its use would not infringe privately-owned rights. Reference herein to any specific commercial product, process, or service by trade name, trademark, manufacturer, or otherwise does not necessarily constitute or imply its endorsement, recommendation, or favoring by the National Technology and Engineering Solutions of Sandia, LLC., the United States Government, or any agency thereof. The views and opinions expressed herein do not necessarily state or reflect those of the National Technology and Engineering Solutions of Sandia, LLC., the United States Government or any agency thereof.

Sandia National Laboratories is a multimission laboratory managed and operated by National Technology and Engineering Solutions of Sandia, LLC., a wholly owned subsidiary of Honeywell International, Inc., for the U.S. Department of Energy's National Nuclear Security Administration under contract DE-NA-0003525.

Parties are allowed to download copies at no cost for internal use within your organization only provided that any copies made are true and accurate. Copies must include a statement acknowledging Sandia's authorship of the subject matter.